Twisted π-Electron System Electrooptic Chromophores. Structural and Electronic Consequences of Relaxing Twist-Inducing Nonbonded Repulsions†

Yiliang Wang,‡ David L. Frattarelli,‡ Antonio Facchetti,‡ Elena Cariati,*,§ Elisa Tordin,§ Renato Ugo,§ Cristiano Zuccaccia,|| Alceo Macchioni,*,|| Staci L. Wegener,‡ Charlotte L. Stern,‡ Mark A. Ratner,*,‡ and Tobin J. Marks*,‡

Department of Chemistry and the Materials Research Center, Northwestern University, 2145 Sheridan Road, Evanston, Illinois 60208-3113, Dipartimento di Chimica Inorganica Metallorganica e Analitica, Università di Milano, Via Venezian 21, I-20133 Milano, Italy, and Dipartimento di Chimica, Università di Perugia, Via Elce di Sotto 8, I-06123 Perugia, Italy

Received: January 13, 2008; Revised Manuscript Received: March 6, 2008

The synthesis, structural and spectroscopic characterization, and nonlinear optical response properties of a "slightly" twisted zwitterionic 4-quinopyran electrooptic chromophore **FMC**, 2-{4-[1-(2-propylheptyl)-1*H*-pyridine-4-ylidene]cyclohexa-2,5-dienylidene}malononitrile, are reported. X-ray diffraction data and density functional theory (DFT) minimized geometries confirm that deletion of the four *o*-, *o*′-, *o*″-, and *o*‴-methyl groups in the parent chromophore **TMC-2**, 2-{4-[3,5-dimethyl-1-(2-propylheptyl)-1*H*-pyridin-4-ylidene]-3,5-dimethylcyclohexa-2,5-dienylidene}malononitrile, relaxes the arene−arene twist angle from 89.6 to 9.0°. These geometrical changes result in a significantly increased contribution of the quinoidal structure to the molecular ground state of **FMC** (versus **TMC-2**), reduced solvatochromic shifts in the optical spectra, and a diminished electric-field-induced second-harmonic (EFISH) generation derived molecular hyperpolarizability ($\mu\beta = -2340 \times 10^{-48}$ esu of DFMC, the dendrimer derivative of **FMC**, vs -24000×10^{-48} esu of **TMC-2**) in CH_2Cl_2 at 1907 nm. Pulsed field gradient spin–echo (PGSE) NMR spectroscopy and EFISH indicate that the levels of **FMC** aggregation in solution are comparable to those of **TMC-2** (monomers and dimers) in CH_2Cl_2 solution. B3LYP and INDO/S computation of chromophore molecular structure, aggregation, and hyperpolarizability trends are in good agreement with experiment.

Introduction

Substitution of organic electrooptic (EO) materials for their inorganic counterparts (e.g., $LiNbO_3$) offers great promise in devices for generating, processing, transmitting, detecting, and storing light signals.[1] Further enhancements of molecule-based EO material properties are expected to greatly facilitate advances in technologies such as optical telecommunications, optical data storage, image reconstruction, and optical computing.[1] Given that molecular/multimolecular chromophores are the active components in organic EO materials, the quest for EO devices with greater bandwidths and lower working voltages will require chromophores having very large molecular hyperpolarizabilities (β), thermal stability, and stable macroscopic noncentrosymmetric alignment. These efforts have constituted a very active research front worldwide for 2 decades.[1]

When designing chromophores with the aforementioned properties, the conventional approach has been to utilize strong terminal electron donor and acceptor substituents, and a planar intervening conjugated π-network.[2] To date, theoretical calculations based on the standard "two-level model" have proven qualitatively successful in predicting β as a function of chromophore geometry and substitution.[3] Here β is determined by three important terms: the difference in dipole moment between the ground and first charge-separated excited electronic state ($\Delta\mu_{ge} = \mu_{ee} - \mu_{gg}$), the transition dipole matrix element connecting these states (μ_{ge}), and an energy gap (ΔE_{ge}) term between these states (eq 1). Taking all of these variables into account, β should, a priori, be tunable via appropriate structural manipulations.

$$\beta \propto \Delta\mu_{ge}(\mu_{ge})^2/(\Delta E_{ge})^2 \quad (1)$$

Currently, several proven molecular design strategies are accepted for enhancing molecular hyperpolarizability.[4] Most commonly employed are those based on extending the π conjugation of planar chromophores, such as "bond length alternation" (BLA)[5] and "auxiliary donors and acceptors".[6] Here, as a result of structural tuning, the hyperpolarizability is enhanced primarily, but not exclusively, by decreasing the energy gap ΔE_{ge} in eq 1. However, large-response chromophores based on extended planar frameworks typically have elaborated molecular structures, creating multistep synthetic challenges, while incurring potential chemical, thermal, and photochemical instabilities. Another drawback of extending planar π conjugated systems is the bathochromic shifts in optical absorption accompanying such π-system extensions. This tendency decreases transparency in the near-IR region where most working wavelengths for photonic devices are found. Other β enhancement strategies for planar chromophores include multidimensional chromophores and zwitterionic chromophores, which have been shown to provide enhanced near-IR transparency, while to some degree sacrificing optimum hyperpolarizability.[7]

It has been argued that all known organic NLO chromophores exhibit only a small fraction (ca. $10^{-3/2}$) of their potential

† Part of the "Larry Dalton Festschrift".

* To whom correspondence should be addressed. E-mail: t-marks@northwestern.edu (T.J.M.).

‡ Northwestern University.

§ Università di Milano.

|| Università di Perugia.

10.1021/jp8003135 CCC: $40.75
Published on Web 05/22/2008

CHART 1: Molecular structures of chromophores TMC-2, TMC-3, FMC, and DFMC

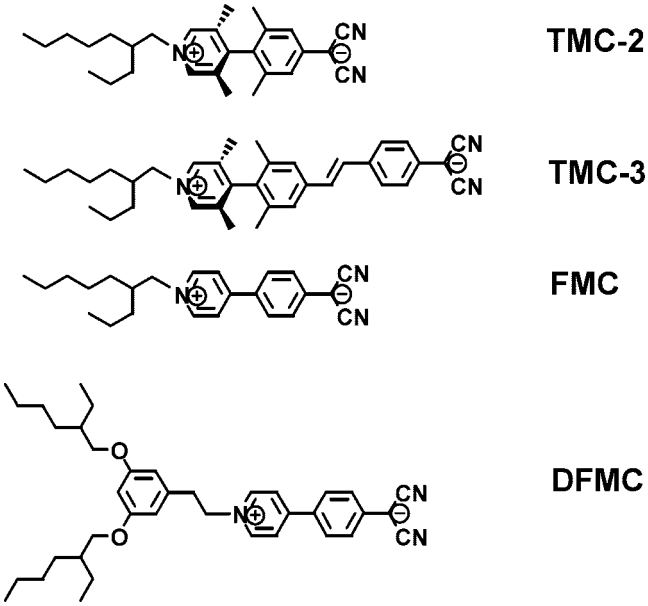

maximum hyperpolarizability,[8] leaving considerable room for developing very large β chromophores not accessible by traditional planar π-system approaches. Computational analysis suggested several years ago that chromophores having unconventional twisted π-systems with charge-separated ground-state structures might exhibit very large first-order hyperpolarizabilities.[9] Since this original proposal, considerable synthetic, spectroscopic, and theoretical attention has been devoted not only to maximizing the molecular response but also to understanding twisted intramolecular charge-transfer (TICT) chromophores from a mechanistic standpoint.[10] As an example, chemically and thermally robust chromophores possessing twisted structures, such as chromophore **TMC-3** (Chart 1),[10c,d] were synthesized, fully characterized, and shown to exhibit ultralarge hyperpolarizabilities, with $\mu\beta$ as large as -488000×10^{-48} esu at 1907 nm. The **TMC-3** figure of merit ($\mu\beta/M_w$) is as large as 945×10^{-48} esu, about 20 times larger than the highest previously reported (46×10^{-48} esu).[1m]

In the detailed structural, spectroscopic, and theoretical studies on first-generation TICT chromophores, it was found that the twisted zwitterionic chromophores have little or no D$-\pi-$A conjugation, thus resulting in charge-localized ground states.[10] The ultralarge hyperpolarizabilities are proposed to arise principally from large dipole moment changes from the molecular zwitterionic ground state to the first excited state, large transition dipole matrix elements, and small ground- to excited-state energetic separations, the latter decreasing markedly in moderately polar solvents such as CH_2Cl_2.[10a,b] In the past, one powerful means to fully understand NLO mechanisms has been to study the relationship between the experimental response and details of the chromophore molecular geometry. At this point, however, our understanding of the twisted π-system chromophores has been largely based on experimental results for sterically crowded, *o*-, *o*′-, *o*″-, and*o*‴-tetramethyl-substituted chromophores such as **TMC-2** and **TMC-3** (Chart 1) where the twist angle is varied over only a small range near 85°. These structures do not provide sufficient data to fully understand the distinctive properties of the ultralarge response molecules, nor test theoretical calculations. Here, in an effort to better understand TICT chromophore structural effects, we report a new chromophore series (**FMC**, **DFMC**; Chart 1) that is structurally similar to **TMC-2**, but designed without *o*-, *o*′-, *o*″-, and *o*‴-methyl substituents, to relax the nonbonded repulsions which impose the large interring twist angle. We report here the synthesis and characterization by X-ray diffraction, solution-phase DC electric-field-induced second-harmonic generation (EFISH), and pulsed field gradient spin–echo (PGSE) NMR spectroscopy of "untwisted" chromophores **FMC** and **DFMC**. These physicochemical results are used in combination with computational analysis to understand chromophore molecular structure, solution-phase aggregation effects, and electrooptic response. It will be seen that such chromophores, with small interring twist angles, have significantly diminished $\mu\beta$ response for reasons that are understandable using quantum chemical models.

Experimental Section

Materials and Methods. All reagents were purchased from Aldrich Chemical Co. and used as received unless otherwise indicated. Tetrahydrofuran (THF) was distilled from sodium/benzophenone and methylene chloride from CaH_2. Toluene was dried by passing through two packed columns of activated alumina and Q_5 under N_2 pressure and regularly tested with benzophenone ketyl in ether solution. The reagent 2-propyl-1-heptanol was purchased from Narchem Co. Solution NMR spectra were recorded on a Varian P-INOVA 500 MHz spectrometer except for PGSE measurements (see below). Elemental analyses were performed by Midwest Microlabs.

(a) Synthesis of 4-(p-Bromophenyl)pyridine (1). To a solution of 1-bromo-4-iodobenzene (1.69 g, 6.00 mmol) in 50 mL of toluene was added the mixture of 4-pyridineboronic acid (0.615 g, 5.00 mmol) in 15 mL of ethanol, followed by the addition of a solution of Na_2CO_3 (1.59 g, 15.0 mmol) in 5 mL of water. This solution was degassed using N_2 for 10 min, and then tetrakis(triphenylphosphine)palladium(0) (0.289 g, 0.25mmol) was added. The resulting reaction mixture was stirred at 110 °C under N_2 overnight. The solvent was then removed using rotary evaporation, and the residue was dissolved in methylene chloride and washed with brine and water. The organic layer was next dried over magnesium sulfate, filtered, concentrated, and purified by silica gel flash column chromatography with an eluent of ethyl acetate:methylene chloride = 1:4 (v/v) to afford 0.957 g (4.1 mmol, 82% yield) of the title compound as a light yellow solid. ^{1}H NMR ($CDCl_3$): δ 8.67 (d, J = 6.0 Hz, 2 H), 7.62 (d, J = 8.0 Hz, 2 H), 7.51 (d, J = 8.0 Hz, 4 H), 7.47 (d, J = 6.0 Hz, 2H).

(b) Synthesis of 2-(4-Pyridin-4-ylphenyl)malononitrile, Sodium Salt (2). To an ice-cooled suspension of NaH (60% mineral oil, 6.72 g, 168 mmol) in anhydrous dimethoxyethane (240 mL) in a three-necked flask under N_2 was added dropwise via syringe, a solution of malononitrile (5.55 g, 84.0 mmol) in anhydrous dimethoxyethane (60 mL). The mixture was stirred for 1 h at room temperature under N_2. Then, **1** (8.82 g, 37.8 mmol) and tetrakis(triphenylphosphine)palladium(0) (4.35 g, 3.76 mmol) were added to the resulting mixture under an N_2 flow. The mixture was then stirred at 85 °C overnight. The solvent was next removed under reduced pressure. The resulting solid was washed with benzene and dried under vacuum, and then was purified via recrystallization from water to afford the title compound as an orange solid (3.40 g, 38% yield). ^{1}H NMR (dimethyl sulfoxide-d_6 (DMSO-d_6)): δ 8.47 (d, J = 6.1 Hz, 2 H), 7.57 (d, J = 6.5 Hz, 2 H), 7.54 (d, J = 8.4 Hz, 4 H), 6.83 (d, J = 7.8 Hz, 2H).

(c) General Procedure for Synthesis of 2-[4-(1-alkyl-1H-pyridine-4-ylidene)cyclohexa-2,5-dienylidene]malononitrile. To a solution of **2** (2.74 g, 11.4 mmol) in 60 mL of anhydrous acetone was added a solution of appropriate alkyl triflate (12.5 mmol) in 60 mL of acetone. The color of the mixture changed from yellow to deep purple immediately. After stirring in the dark at room temperature overnight, the solvent was removed under reduced pressure. The resulting solid was dissolved in methylene chloride and washed with brine and water. The organic layer was then dried over magnesium sulfate, filtered, concentrated, and purified by silica gel flash column chromatography with a gradient eluent of 2−4% (volume) of methanol in methylene chloride to afford the various title compounds.

(d) Synthesis of 2-{4-[1-(2-propylheptyl)-1H-pyridin-4-ylidene]cyclohexa-2,5-dienylidene}malononitrile (3). Compound **3** was obtained as a purple solid (53% yield). ^{1}H NMR ($CDCl_3$):[11] δ 7.98 (d, J = 6.8 Hz, 2 H), 7.52 (d, J = 7.0 Hz, 2 H), 7.20 (d, J = 8.8 Hz, 4 H), 6.71 (d, J = 8.8 Hz, 2H), 4.27 (d, J = 7.9 Hz, 2H), 1.93 (m, 1H), 1.2−1.4 (m, 12H), 0.90 (m, 6H). MS (high resolution, EI): m/z 360.2441 $[M + H]^+$; calcd, 360.2439. Anal. Calcd for $C_{24}H_{29}N_3$: C, 80.18; H, 8.13; N, 11.69. Found: C, 79.80; H, 7.91; N, 11.47.

(e) Synthesis of 2-[4-(1-{2-[3,5-Bis(2-ethylhexyloxy)phenyl-]ethyl}-1H-pyridin-4-ylidene)cyclohexa-2,5-dienylidene]malononitrile (4). Compound **4** was obtained as a brown-red solid (60% yield). ^{1}H NMR ($CDCl_3$):[11] δ 7.77 (d, J = 8.1 Hz, 2 H), 7.40 (d, J = 7.7 Hz, 2 H), 7.13 (d, J = 8.8 Hz, 4 H), 6.66 (d, J = 8.8 Hz, 2H), 6.34 (t, J = 1.8 Hz, 1H), 6.11 (d, J = 1.8 Hz, 2H), 4.59 (t, J = 6.9 Hz, 2H), 3.71 (m, 4H), 3.11 (t, J = 6.1 Hz, 2H), 1.64 (m, 2 H), 1.5 – 1.2 (m, 16 H), 0.88 (m, 12 H). MS (high resolution, EI): m/z 580.3894 $[M + H]^+$; calcd, 580.3903. Anal. Calcd for $C_{38}H_{49}N_3O_2$: C, 78.72; H, 8.52; N, 7.25. Found: C, 78.91; H, 8.60; N, 7.03.

(f) Synthesis of Methyl 2-(3,5-Bis(2-ethylhexyloxy)phenyl)-acetate (5). A mixture of methyl 2-(3,5-dihydroxyphenyl)acetate (911 mg, 5.00 mmol), 2-ethylhexyl bromide (2.10 mL, 11.7 mmol), anhydrous K_2CO_3 (2.00 g, 14.5 mmol), and 18-crown-6 (300 mg, 1.13 mmol) in acetone (20 mL) was refluxed for 3 days. Acetone was then removed using rotary evaporation, and the residue was extracted with hexanes and washed with water. The organic layer was dried over anhydrous magnesium sulfate, filtered, evaporated, and purified by silica gel flash column chromatography with an eluent of hexanes:dichloromethane = 3:1 (v/v) to afford 1.83 g (90% yield) of colorless viscous oil, **5**. ^{1}H NMR ($CDCl_3$): δ 6.41 (s, 2 H), 6.37 (s, 1 H), 3.80 (d, J = 4.4 Hz, 4 H), 3.70 (s, 3 H), 3.54 (s, 2 H), 1.69 (m, 2 H), 1.2−1.6 (m, 16 H), 0.92 (t, J = 6.4 Hz, 12 H).

(g) Synthesis 2-(3,5-Bis(2-ethylhexyloxy)phenyl)ethanol (6). To a suspension of $LiAlH_4$ (270 mg, 7.11 mmol) in anhydrous THF (10 mL) was added dropwise a solution of methyl 2-(3,5-bis(2-ethylhexyloxy)phenyl)acetate (1.92 g, 4.73 mmol) in anhydrous THF (5 mL) at room temperature. The resulting reaction mixture was stirred for another 1.5 h and then carefully quenched with ethyl acetate, followed by water. Dilute HCl(aq) was added to dissolve the aluminum salts, and the product was extracted with ethyl acetate and washed with water. The organic layer was dried over anhydrous magnesium sulfate, filtered, evaporated, and purified by silica gel flash column chromatography with an eluent of methylene chloride to afford 1.78 g (99%) of colorless viscous oil, **6**. ^{1}H NMR ($CDCl_3$): δ 6.36 (s, 2 H), 6.35 (s, 1 H), 3.86 (t, J = 6.4 Hz, 2 H), 3.81 (d, J = 5.2 Hz, 4 H), 2.80 (t, J = 6.8 Hz, 2 H), 1.70 (m, 2 H), 1.2−1.6 (m, 16 H), 0.92 (t, J = 6.4 Hz, 12 H).

(h) Synthesis of 3,5-Bis(2-ethylhexyloxy)phenethyl trifluoromethanesulfonate (7). To a solution of **6** (1.40 g, 3.70 mmol) in anhydrous methylene chloride (30 mL) was added dropwise triflic anhydride (0.820 mL, 4.87 mmol) in anhydrous methylene chloride (7 mL) at room temperature. The solution was stirred for another 2 h and poured into crushed ice. The mixture was then neutralized with saturated aqueous $NaHCO_3$ solution. The product was next extracted with ethyl acetate and washed with water. The organic layer was dried over anhydrous magnesium sulfate, filtered, evaporated, and purified by silica gel flash column chromatography with an eluent of dichloromethane to afford 1.80 g (96% yield) of light brown viscous oil, **7**. ^{1}H NMR ($CDCl_3$): δ 6.38 (s, 1 H), 6.33 (s, 2 H), 4.68 (t, J = 7.0 Hz, 2 H), 3.80 (m, 4 H), 3.05 (t, J = 7.0 Hz, 2 H), 1.70 (m, 2 H), 1.2−1.6 (m, 16 H), 0.92 (m, 12 H).

Optical Spectroscopy. Optical spectra were recorded on a Cary 5000 spectrophotometer. Dilute solutions (10^{-5} M) of chromophores in various solvents were prepared to study solvent effects on chromophore optical absorption. Variable-concentration measurements at higher concentrations for intermolecular aggregation studies were not feasible due to the strong extinction coefficients.

Single-Crystal X-ray Diffraction. Single crystals of **FMC** were obtained via slow vapor diffusion. A small vial containing a solution of **FMC** in methylene chloride was placed in a closed chamber, into which diethyl ether was added. The small vial was sealed with a plastic cap having a small hole to allow the slow diffusion of diethyl ether vapor from the chamber into the vial for single-crystal growth. All diffraction measurements were carried out on a Bruker SMART CCD diffractometer with graphite-monochromated Mo Kα (0.71073 Å) radiation. Data were collected using the Bruker SMART detector, processed using the SAINT-NT package from Bruker, and corrected for Lorentz and polarization effects. The structure was solved using direct methods (SHELXTL-90) and expanded using Fourier techniques (SHELXTL-97). The non-hydrogen atoms were refined anisotropically, with the exception of several disordered 2-propylheptyl carbon atoms which were refined with group anisotropic displacement parameters. Hydrogen atoms were included in idealized positions but not refined. All calculations were performed using the Bruker SHELXTL9 crystallographic software package. Crystallographic parameters are summarized in Tables S1−S5 of the Supporting Information.

Pulsed Field Gradient Spin–Echo NMR Spectroscopy. Intermolecular aggregation was quantitatively analyzed using PGSE NMR spectroscopy. ^{1}H PGSE NMR measurements were performed at 295.7 K without spinning by using the standard stimulated echo pulse sequence[12] on a Bruker AVANCE DRX 400 spectrometer equipped with a GREAT 1/10 gradient unit and a QNP probe with a Z-gradient coil. The shape of the gradients was rectangular, their duration (δ) was 4 ms, and their strength (G) was varied during the experiments. All spectra were acquired using 32K points and a spectral width of 5000 Hz and were processed with a line broadening of 1.0 Hz. Different values of "nt" (number of transients) and numbers of different gradient strengths (G) were used for different samples, depending on solution viscosity and solute concentration. The dependence of the resonance intensity (I) on a constant diffusion time and on a varied G is described by eq 2:

$$\ln\frac{I}{I_0} = -(\gamma\delta)^2 D_t\left(\Delta - \frac{\delta}{3}\right)G^2 \qquad (2)$$

where I = intensity of the observed spin–echo, I_0 = intensity of the spin–echo without gradients, D_t = diffusion coefficient, Δ = delay between the midpoints of the gradients, and δ =

CHART 2: (A) Chemical structures of computationally analyzed chromophores. Computed arene−arene dihedral twist angles are given in parentheses. (B) Structural model for centrosymmetric chromophore dimers, the energetics of which were examined computationally as a function of interplanar spacing along the *z* axis

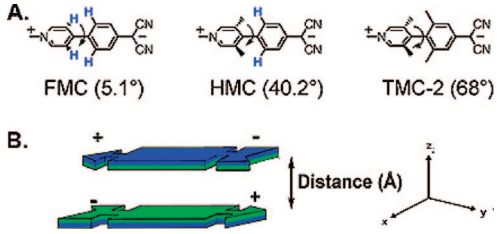

length of the gradient pulse, and γ = magnetogyric ratio. The semilogarithmic plots of $\ln(I/I_0)$ vs G^2 were fitted using the standard linear regression algorithm implemented in the Origin 7 software package; the *R* factor was always greater than 0.99. For pure solvents, the diffusion coefficient D_t, which is directly proportional to the slope of the regression line obtained by plotting $\log(I/I_0)$ vs G,[2] was estimated by measuring the proportionality constant using an HDO sample (0.04%) in D_2O (known diffusion coefficient in the range of 274–318 K)[13] under the exact same conditions as the sample of interest [$D_t(CD_2Cl_2) = 33.2 \times 10^{-10}$ m^2 s^{-1}, D_t(DMSO-d_6) = 6.5×10^{-10} m^2 s^{-1}]. Solvents were used as internal standards to account for possible changes in solution viscosity,[14] temperature, and gradient strength.[15] The experimental error in D_t was estimated to be 3% for all solutions except those with concentration values smaller than 10^{-5} M. In such cases, the error can approach 5–8%.

EFISH Measurements. Measurements of $\mu\beta$, the products of the chromophore dipole moment (μ) and the projection of β_{VEC}, the vector part of the molecular first-order hyperpolarizability β tensor along the direction of $\boldsymbol{\mu}$, were performed by the solution-phase DC EFISH generation method. EFISH measurements were carried out in CH_2Cl_2 solutions at a nonresonant fundamental wavelength of 1907 nm using a Q-switched, mode-locked Nd^{3+}:YAG laser [pulse durations of 15 ns (90 ns) at a 10 Hz repetition rate]. The 1064 nm initial wavelength was shifted to 1907 nm by a Raman shifter with a high-pressure H_2 cell.[10c,d] CH_2Cl_2 was freshly distilled from P_2O_5. The organic base 1,4-diazabicyclo[2.2.2]octane (DABCO; molar ratio DABCO:chromophore = 0.5:1.0) was added to the solutions to increase chromophore stability.

Computational Methodology. ***(a) Gas-Phase Electronic Structure.*** Three model monomers were used for addressing response-dependent relationships associated with sterically induced modification of the twist angle: **FMC**, **HMC**, and **TMC** (Chart 2A). Geometries were obtained at the B3LYP level[16,17] in Jaguar[16] v5.00.22 using the Maestro Molecular Modeling Interface c5.10.20 and a 6-31G** basis set. In several previous studies of TICT chromophores, this methodology has yielded results in good agreement with experimental data.[9,10b]

(b) Gas-Phase Dimerization Analysis. The quinopyran chromophores **FMC**, **HMC**, and **TMC-2** were examined for intermolecular aggregation as density functional theory (DFT)-minimized centrosymmetric eclipsed dimers using the Spartan[18] software package (Chart 2B). Starting with centrosymmetric model structures for **FMC**, **HMC**, and **TMC-2**, each chromophore pair was separated in a stepwise fashion, starting from the DFT-minimized pair geometry. By adjusting the center-to-center interplanar distance in one direction, single-point energies were computed in finite intervals along the *z*-axis, as shown in Chart 2B, at the restricted Hartree–Fock level with a 3-21G* basis set within Spartan. To simplify the calculation further, it was assumed that upon increase in interplanar separation, no further molecular structural changes occur. From this analysis we obtained dimer distance-dependent energies (E_D; Figure 7). Using both E_D and monomer energies (E_M), the ΔE_D was calculated by via eq 3.

$$\Delta E_D = E_D - 2(E_M) \tag{3}$$

The difference in the energy associated with the FMC and TMC-2 dimer pairs is then given by eq 4.

$$\Delta E_{diff}^{D} = \Delta E_D^{FMC} - \Delta E_D^{TMC\text{-}2} \tag{4}$$

(c) Solution-Phase Calculations. To provide a more accurate estimate of solvent effects on monomer and dimer energetics, initial DFT structures were used in single-point RHF continuum-solvation calculations by solving the Poisson–Boltzmann (PB) equation numerically within the Jaguar[16] package (Figure 7).[19] This involves the numerical solution of the PB equation to determine the self-consistent reaction field (SCRF) of the solvent acting on the quantum mechanical solute. In this approach, the solute is either monomeric **FMC** or **TMC-2** or their corresponding dimers immersed in a continuum solvent characterized by four properties: the solvent probe radius (r_{probe} = 2.33 for CH_2Cl_2), the solvent dielectric constant ($\varepsilon_{solvent}$ = 9.08), the solvent molecular weight (MW = 84.93), and the solvent density (d = 1.326). CH_2Cl_2 was chosen since it was used extensively in the PGSE and EFISH experiments. PB RHF single-point solvation energies (E_{sol}) were then computed for the monomers (E_{sol}^{M}) and dimers (E_{sol}^{D}) of each molecule. This computation gives the dimer pair solvation energy correction term (ΔE_{sol}^{corr}) as in eq 5.

$$\Delta E_{sol}^{corr} = E_{sol}^{D} - 2\left(E_{sol}^{M}\right) \tag{5}$$

With the effect of solvation and/or dimerization (ΔE_{sol}^{corr}) for each molecule calculated, these values were then used to correct for solvation in the gas-phase evaluations of the equilibrium structure dimers (those having the shortest interplanar separation) to give total environmental stabilization energies versus the nonsolvated monomers (ΔE_{sta}). These were determined from the expression in eq 6.

$$\Delta E_{sta} = \Delta E_D + \Delta E_{sol}^{corr} \tag{6}$$

(d) Semiempirical INDO/S[20] CI Calculations. Semiempirical calculations employing the INDO/S[20] model developed by Zerner and co-workers were also performed using the CNDO[21] program. INDO/S at the monoexcited CI level provided the linear spectral properties and excitations necessary for the hyperpolarizability calculations. To better understand solvent-dependent response changes associated with CH_2Cl_2 (used in the EFISH and PGSE experiments), additional calculations were implemented in which a simple dipolar field (F = 0.006 au) was applied along the longitudinal molecular axis defined by the interphenyl bond (z direction). This external field mimics the effect of solvent polarization on the isolated chromophore.[20] During each of the monoexcited CI calculations, an active space of 70 × 70 was used.

(e) Hyperpolarazibility Calculations. From the INDO/S[20] output, the sum-over-states[22] (SOS) approach was implemented to evaluate the molecular nonlinear responses (β) of the three chromophores; the states involved came from a 70 × 70 set of single excitations. The hyperpolarizability (β) appears as the third rank tensor in the first nonlinear term that arises in the

SCHEME 1: Synthesis of Reduced Twist Angle Chromophores

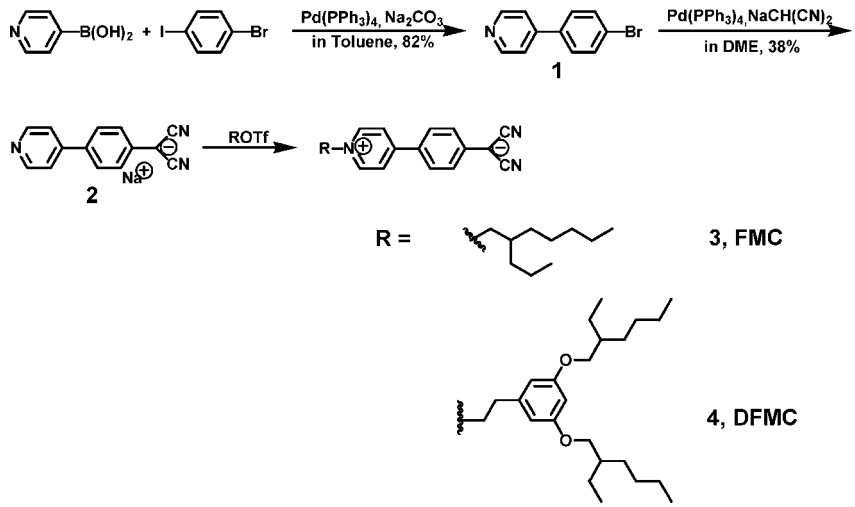

dependence of the molecular induced dipole moment (μ) on the applied electric field F experienced by the molecule (eq 7).

$$\mu_i = \mu_i^{(0)} + \sum_i \alpha_{ij} F_j + 1/2 \sum_{j,k} \beta_{ijk} F_j F_k \tag{7}$$

Here $\mu_i^{(0)}$ is the permanent dipole moment of the molecule in direction i, F_j is the component of the electromagnetic field in direction j, and α and β are the static (zero frequency, $\omega = 0.0$ eV) first- and second-order polarizability tensors. We concentrate here on β. To avoid issues of resonance enhancement, we report only the limiting zero frequency or "static" case ($\omega = 0.0$ eV). We are interested in the β_μ (β_{VEC}) component of the β tensor (eq 8):

$$\beta_\mu = \frac{\sum_{i=x,y,z} \beta_i \mu_i}{||\mu||} \qquad \beta_i = \frac{1}{3} \sum_{k=x,y,z} (\beta_{ikk} + \beta_{kik} + \beta_{kki}) \tag{8}$$

As has been discussed elsewhere,[10a] the use of simple INDO/S SOS is not extremely accurate for calculating the response properties of TICT chromophores. We use it here only to support and interpret trends in the nonlinear response.

Results

In the following discussion, we present physicochemical data combined with theoretical calculations aimed at analyzing and understanding the effects of reduced interring twist angle on zwitterionic TICT chromophore EO response. We begin with a discussion of synthetic strategies for **FMC/DFMC** chromophore preparation and then focus on solution and solid-state structural characterization, including comparison with the TICT structure of **TMC-2**. We then discuss solution optical spectra and solvatochromism as revealed by the solvent dependence of the spectra. Chromophore aggregation is then assayed by PGSE NMR spectroscopy and compared to that in **TMC-2**. Next, EFISH spectroscopy in solution is employed to quantify **FMC/DFMC** chromophore hyperpolarizability and to compare it with the *o*,*o*′,*o*″,*o*‴-tetramethyl-TICT chromophore response. Finally, a computational analysis of interring twist angle effects on hyperpolarizability and chromophore aggregation is carried out, and the results are compared with experiment.

Chromophore Synthetic Approaches. The straightforward synthetic pathways to reduced twist angle chromophore **FMC** and its dendron derivative **DFMC** (for greater solubility) are summarized in Schemes 1 and 2, respectively. Building block **1** is synthesized via Suzuki coupling of commercially available 4-pyridineboronic acid and 1-bromo-4-iodobenzene in high yield (82%). Pd-catalyzed coupling of **1** with sodium dicyanomethanide then affords sodium salt **2** in acceptable yield (38%). This intermediate is then regioselectively N-alkylated with the appropriate alkyl triflates to afford chromophores **FMC** and **DFMC**. The synthesis of the dendrimeric alkyl triflate subsituent for **DFMC** (Scheme 2) begins with commercially available methyl 3,5-dihydroxylphenylacetate, which undergoes 18-crown-6-catalyzed alkylation with 1-bromo-2-ethylhexane to afford dialkoxy compound **5**, in high yield (90%). Near-quantitative reduction of **5** using $LiAlH_4$ gives alcohol **6**, which is then treated with triflic anhydride to afford dendrimenric alkyl triflate **7** in very high yield (96%).

Chromophores **FMC** and **DFMC** are characterized by high-resolution mass spectroscopy, elemental analysis, ^{1}H NMR spectroscopy, and, in the case of **FMC**, single-crystal X-ray diffraction. Details are compiled in the Experimental Section.

Solid-State Structure of Chromophore FMC. Chromophore **FMC** is found to belong to crystallographic space group $P\bar{1}$. Disorder in the 2-propylheptyl substituent prevents optimum structural refinement; however, the metrical parameters were obtained with sufficient accuracy to discern important bond distance and angle trends, which are summarized in Table 1. Metrical data for **TMC-2** are also presented here for comparison. The molecular structure of **FMC** is shown in Figure 1.

Compared to the diffraction-derived arene dihedral twist angle in **TMC-2** of 89.6°, **FMC** exhibits a much smaller twist angle of 9.0°. In addition, the (ring)C−C(ring) distance in **FMC** (C9−C10 = 1.449(6) Å) is also significantly shorter than in **TMC-2** (1.488(5) Å), as is the (ring)C−C(CN)$_2$ distance. Furthermore, the internal arene distances C11−C13 = 1.346(6) Å, C12−C14 = 1.360(6) Å, C5−C7 = 1.364(6) Å, and C6−C8 = 1.360(6) Å appear to be significantly shorter than the corresponding distances in **TMC-2** of 1.369(5), 1.373(5), 1.390(5), and 1.390(5) Å, respectively.

These differences between the crystal structures of **FMC** and **TMC-2** are doubtless an indication of the change in electronic structures of these TICT chromophores with sterically induced changes in ring–ring twist angle. The relative contributions of two possible resonance hybrids, zwitterionic and quinoidal, to the TICT chromophore ground states explain the observed

SCHEME 2: Synthesis of Dendrimeric Alkyl Triflate for DFMC Preparation

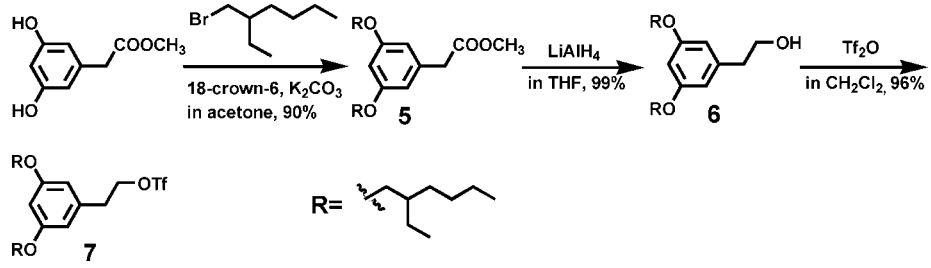

TABLE 1: Important Diffraction-Derived Metrical Parameters for Chromophores FMC and TMC-2

chromophore	twist angle (deg)	ipso (ring)C−C (ring) (Å)	(ring)C−C $(CN)_2$ (Å)
FMC	9.0	1.449(6)	1.429(6)
TMC-2[a]	89.6	1.488(5)	1.463(5)

[a] From refs 10c and 10d.

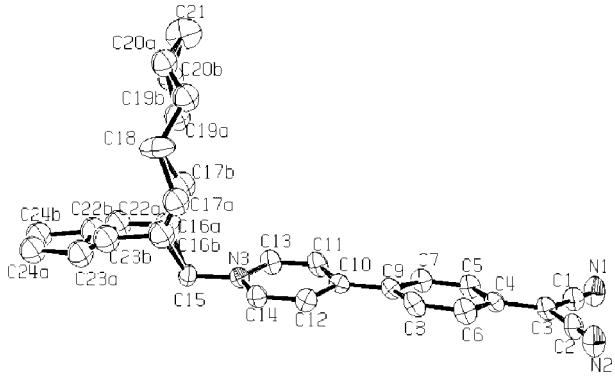

Figure 1. ORTEP drawing (50% probability elipsoids) of chromophore **FMC**. Hydrogen atoms and solvent molecules have been omitted for clarity. Several carbon atoms on the *N*-alkyl chain are disordered.

SCHEME 3: Contributing Zwitterionic (Left) and Quinoidal (Right) Resonance Structures of TICT Chromophores: R = -CH_3 for TMC-2 and R = H for FMC

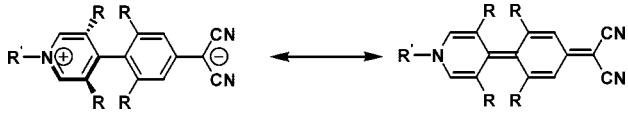

differences in metrical parameters (Scheme 3). The changes in molecular structure are expected to lead to changes in relative fractions of the contributions from the two contributing resonance structures and, concomitantly, to changes in electronic structure. In **TMC-2**, nonbonded repulsions among the *o*-, *o*′-, *o*″-, and *o*‴-methyl substituents forces a nearly perpendicular arene−arene twist angle. The result is pronounced reduction in interring conjugation, reduced intramolecular charge transfer, and a dominant ground-state zwitterionic structure. However, in **FMC**, with minimal *o*, *o*′, *o*″, and *o*‴ nonbonded repulsions, intramolecular charge transfer is greatly enhanced due to molecular near-planarity and effective interring conjugation. Thus, the contribution from the quinoidal structure is increased in the ground state, as assessed by the greater double bond character in the (ring)C−C(ring), (ring)C−C$(CN)_2$, and other intraring C−C bond distances. This result is in good accord with other data (see below).

Optical Spectroscopy. FMC and **DFMC** exhibit rather similar optical spectra, both evidencing negative solvatochromic shifts (Figure 2), reminiscent of those for twisted chromophore **TMC-2**, but with larger extinction coefficients.[10c,d] The **FMC** and **DFMC** charge-transfer bands exhibit large blue shifts with increased solvent polarity (Table 2), strongly indicating a more polar ground state. Note however from the data in Table 2 that the solvatochromic shift is significantly greater for twisted chromophore **TMC-2**, indicating smaller changes in the dipole moment from the ground state to the first charge-transfer excited state in the more planar, more quinoidal **FMC** and **DFMC** chromophores.

PGSE NMR Spectroscopic Analysis of Chromophore Aggregation. PGSE NMR is a powerful tool to provide quantitative information on solution-phase chromophore aggregation. PGSE NMR experiments are used here to estimate the molecular dimensions and level of aggregation of chromophores **FMC** and **DFMC** in solution. The procedural precautions, described recently,[23] were followed here for treating the diffusion data. Diffusion coefficients (D_t) as a function of

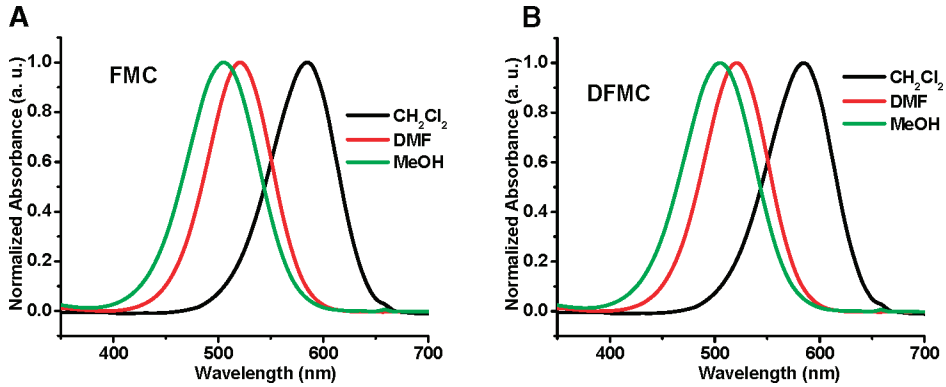

Figure 2. Optical absorption spectra of chromophores **FMC** (A) and **DFMC** (B) as a function of solvent polarity. Only interfragment CT bands are shown here. Dilute solutions (10^{-5} M) of the chromophores in various solvents are used in these experiments. The spectra have been smoothed using the Savitzky−Golay filter method.

TABLE 2: Optical Absorption (λ_{max}, nm, and Extinction Coefficient ε, M^{-1} cm^{-1}) Data and Estimated Changes in Dipole Moment ($\Delta\mu$, 10^{-30} C·m) from the Ground to First Excited State for Chromophores FMC and DFMC in Selected Solvents

	λ_{max} (ε)[a]		
solvent (E_T)	TMC-2[b]	FMC	DFMC
CH_2Cl_2 (0.31)	556 (1840)	582 (63900)	585 (62100)
DMF (0.40)		520	521
MeOH (0.76)	440	503	505
$\Delta\mu$[c]	−21.4	−6.5	−6.5

[a] Assigned to a low-energy inter-subfragment charge-transfer (CT) excitation. [b] From refs 10c and 10d. [c] DFT-derived change in dipole moment from ground to excited state.

TABLE 3: Diffusion Coefficients ($10^{10}D_t$, m^2 s^{-1}), Structure Parameters (P, Å), and Aggregation Numbers (N)[a] for Chromophores FMC, DFMC, and TMC-2 as a Function of Concentration and Solvent

entries		C (mM)	D_t	P	N
		FMC			
1	CD_2Cl_2	0.23	10.07	30.34	1.06 ± 0.03
2	CD_2Cl_2	0.76	9.68	31.53	1.14 ± 0.06
3	CD_2Cl_2	2.17	9.16	33.35	1.27 ± 0.09
4	CD_2Cl_2	3.57	9.03	33.81	1.34 ± 0.10
5	CD_2Cl_2	7.80	8.55	35.72	1.46 ± 0.11
6	CD_2Cl_2	15.12	8.31	36.75	1.56 ± 0.11
7	CD_2Cl_2	18.72	8.06	37.88	1.59 ± 0.10
8	DMSO	0.15	2.15	28.21	
9	DMSO	0.75	2.12	28.74	
10	DMSO	4.45	2.06	29.47	
11	DMSO	12.15	2.05	29.65	
		DFMC			
12	CD_2Cl_2	0.108	7.98	38.24	1.03 ± 0.01
13	CD_2Cl_2	0.13	7.96	38.35	1.03 ± 0.01
14	CD_2Cl_2	0.63	7.68	39.77	1.09 ± 0.01
15	CD_2Cl_2	0.90	7.63	39.99	1.12 ± 0.03
16	CD_2Cl_2	1.76	7.39	41.33	1.19 ± 0.03
17	CD_2Cl_2	3.18	7.05	43.31	1.26 ± 0.05
18	CD_2Cl_2	5.90	6.76	45.19	1.35 ± 0.06
19	CD_2Cl_2	7.42	6.72	45.42	1.38 ± 0.06
20	CD_2Cl_2	12.16	6.52	46.82	1.46 ± 0.06
21	DMSO	0.35	1.62	37.56	
22	DMSO	1.67	1.60	37.88	
23	DMSO	3.08	1.61	37.70	
		TMC-2[b]			
24	CD_2Cl_2	0.006	10.06	30.36	1.00 ± 0.01
25	CD_2Cl_2	0.07	9.32	32.77	1.01 ± 0.02
26	CD_2Cl_2	0.50	9.05	33.72	1.08 ± 0.08
27	CD_2Cl_2	1.60	8.52	35.84	1.18 ± 0.13
28	CD_2Cl_2	4.00	7.77	39.26	1.30 ± 0.15
29	CD_2Cl_2	8.40	7.30	41.81	1.41 ± 0.14
30	DMSO	0.05	1.99	30.61	
31	DMSO	0.34	1.94	31.33	
32	DMSO	4.83	1.95	31.15	

[a] Calculated according to eq 13. The error intervals on N are reported at 95% confidence. [b] From refs 10c and 10d.

concentration were measured at 295.7 K for **FMC** and **DFMC** in CD_2Cl_2 and DMSO and contrasted with those previously obtained for **TMC-2** (Table 3).[10c,d] From D_t values, the hydrodynamic dimensions of the diffusing particles, assumed to have ellipsoidal shapes, were derived by applying the modified Stokes–Einstein (eq 9):[23]

$$D_t = \frac{kT}{f_s c \pi \eta \sqrt[3]{ab^2}} \quad (9)$$

Here k is the Boltzman constant, T is the absolute temperature, η is the fluid viscosity, c is the "size factor", which depends on the ratio between the radius of the solvent and that of the diffusing particle, f_s is the "shape factor", and a and b are the major and minor semiaxes of the ellipsoid, respectively. The dependence of f_s on a and b for prolate or oblate ellipsoids is known.[23] Structure parameter P (eq 10)

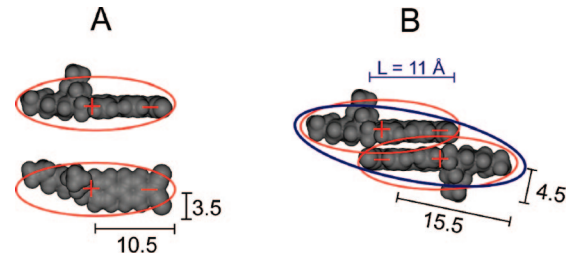

Figure 3. Monomer (A) and dimer (B) van der Waals surfaces of the **FMC** chromophore. Ellipsoids used as geometrical models for PGSE NMR data analysis are depicted in red (monomer) and blue (dimer).

$$P = kT/\pi\eta D_t = f_s c \sqrt[3]{ab^2} \quad (10)$$

is derived from the known values of η and T and the measured D_t values (Table 3).

The aggregation numbers N (the average number of monomer units in an aggregate) were calculated via eq 13 (see below) and are seen to significantly diverge from unity (Table 3), indicating that all three chromophores are to some extent associated in CD_2Cl_2. Nevertheless, N never approaches 2, which would correspond to the predominance of dimers. Assuming that: (i) self-aggregation is limited to a monomer–dimer equilibrium and (ii) both monomer and dimer have prolate ellipsoidal shapes, the dimerization equilibrium constant (K_D) can be estimated by fitting the experimental trends of P vs concentration, C, with an appropriate expression (eq 11).

$$P = x_M P_M + x_D P_D \quad (11)$$

Here x_M and x_D are the mole fractions of the monomer and dimer, respectively, which can be expressed as a function of K_D and C (eq 12):[23]

$$x_M = 2 - \frac{2C}{C + \frac{\sqrt{1 + 8K_D C} - 1}{4K_D}} \quad \text{and} \quad x_D = 1 - x_M \quad (12)$$

Parameters P_M and P_D depend on the semiaxes of the ellipsoids (a_M, a_D, b_M, and b_D) and r_{solv}. The latter can be considered approximately equal to the van der Waals radius of CD_2Cl_2 (r_{solv} = 2.49 Å). Some structural hypotheses must be made as far as the a and b parameters are concerned. The case of chromophore **FMC** is examined in detail. **FMC** is treated as a prolate ellipsoid having the major axis ($2a_M$) equal to 21 Å (approximately the distance between the terminal CH_3 group and the nitrogen of the CN moiety in the conformer having a fully elongated alkyl chain, Figure 3A). The minor semiaxis (b_M, 3.5 Å) can be derived (Figure 3A) from the experimentally determined P_M value in DMSO (29.02 Å), reasonably assuming that only monomers are present in such a polar solvent.

Having estimated a_M and b_M, the theoretical value of P_M in CD_2Cl_2 is derived (29.47 Å). Experimental P data in CD_2Cl_2 as a function of C are then fitted using eq 11 in which P_M is set equal to 29.47 Å, while K_D and P_D are the parameters to determine (Figure 4, black squares). The best fit gives K_D = 293 ± 149 M^{-1} and P_D = 43.13 ± 2.27 Å.

Reasonably assuming that two monomers stack in an anti-parallel fashion, minimizing the distance between positive and negative charges with an overlap region (L) along the major

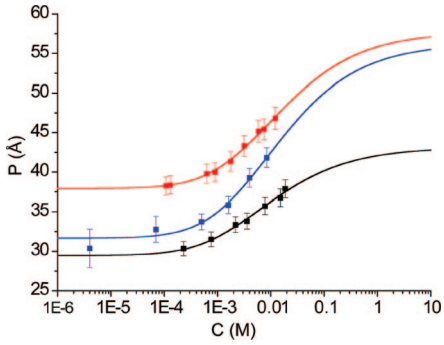

Figure 4. Experimental P values as a function of concentration for chromophore **FMC** (black), **DMFC** (red), and **TMC-2** (blue) in CD_2Cl_2 (where, for example, 1E-6 represents 1×10^{-6}). Solid lines are best fits to the data using eq 11.

axis of ~11 Å (Figure 3B), yields $a_D = 15.5$ Å. Consequently, from P_D (43.13 Å), b_D is estimated to be 4.5 Å. The same procedure was applied to the **DFMC** and **TMC-2** data to yield the results in Table 4.

Note that the minor semiaxis of monomer (b_M) slightly increases on passing from **FMC** to **TMC-2** and **DFMC**. Also, the minor semiaxis of the dimer (b_D) increases in the series **FMC**, **DFMC**, and **TMC-2**. The relative increment is much larger on passing from **FMC** to **TMC-2** since the *o*-methyl groups in the twisted **TMC-2** chromophore impede closer approach of two molecules. Note that the dimerization equilibrium constants (K_Ds) of the three chromophores are not significantly different, varying from 200 to 300 M^{-1} (−13 kJ $mol^{-1} < \Delta G_D°(296) < -14$ kJ mol^{-1}). From the K_D values, Ns can be computed at each concentration according to eq 13 (Table 3).[23]

$$N = \frac{2C}{C + \dfrac{\sqrt{1 + 8K_D C} - 1}{4K_D}} \qquad (13)$$

EFISH Measurements. Concentration-dependent EFISH experiments were used to measure $\mu\beta$ values of chromophores **FMC** and **DFMC** and their intermolecular aggregation in CH_2Cl_2. The results are summarized in Table 5, where it can be seen that **FMC** and **DFMC** have negative $\mu\beta$ responses, as does **TMC-2**.[10c,d] Dendrimer-functionalized **DFMC** $\mu\beta$ values are used here to compare with those of **TMC-2**. Assuming that the "full" molecular $\mu\beta$ value is obtained in the concentration range where the response is no longer concentration-dependent, the $\mu\beta$ value of **DFMC** is found to be $(-2340 \pm 330) \times 10^{-48}$ esu in CH_2Cl_2 at 5×10^{-4} M, only about one-tenth of the $\mu\beta$ of the twisted analogue **TMC-2** ($(-24000 \pm 2400) \times 10^{-48}$ esu in CH_2Cl_2 at 5×10^{-6} M). Chromophore **FMC** has a response comparable to that of **DFMC**. Similar to that of chromophore **TMC-2**, **FMC** and **DFMC** $\mu\beta$ values are highly concentration-dependent, due to the aggregation effects (see more below).

Theoretical Analysis. Two issues related to chromophore response properties were examined: (1) molecular electronic structure and hyperpolarizability as a function of increasing chromophore *o*-methyl substitution (Scheme 1; chromophores **FMC**, **HMC**, and **TMC-2**), hence twist angle (see Experimental Section for details of the computational procedures); (2) aggregation tendencies as a function of substitution. Regarding issue 1, Table 6 shows that the computed ground-state arene−arene twist angle increases from 5.1 to 40.2 to 68° with the incorporation of zero, two, and four methyl groups, respectively, ortho to the arene−arene juncture.

Note that better theoretical and experimental agreement (Table 5 and Table 7) is obtained when a dipolar field (CH_2Cl_2, $F = 0.006$ au, representing very crudely the effect of solvent polarization) was applied, resulting in a more stable zwitterionic state and enhanced response.

It is also found that increasing twist angle gives rise to a concomitant increase in the computed ipso (ring)C−C(ring) and (ring)C−$C(CN)_2$ bond distances, in good agreement with the crystal structure data (Table 1 and Table 8). Moreover, with this structural progression and increasing dominance of a diradicaloid or zwitterionic[10a,b,c] ground state, the hyperpolarizability is found to increase substantially due to the increase in change in dipole moment and the decrease in energy separating the zwitterionic ground state and first excited state, as expected using the two-level model (Table 6).

These trends can be understood more completely by considering the HOMO and LUMO spatial distributions for the three chromophores (Figure 5). The HOMO is seen to be increasingly localized on the dicyano methylene group in the progression from **FMC** to **TMC-2**, and the LUMO is found to exhibit the opposite trend with increasing localization on the pyridium cation. Note that the HOMO is destabilized by 0.66 eV in progressing from **FMC** to **TMC-2**, while the LUMO is stabilized by −0.31 eV. It is found that planarization of **TMC-2** by removing *o*-methyl substituents in **FMC** increases the quinoidal resonance contribution and the HOMO−LUMO gap (3.69 vs 4.65 eV, respectively). Lastly, it is found that not only the computed $\mu\beta$ values decline at zero frequency with the **TMC-2** → **FMC** progression but $\mu\beta$ also increases in the presence of a dipole field for all respective chromophores, finding acceptable agreement with experiment.[10c]

Results for issue 2 are plotted in Figure 6, which examines unsolvated chromphore dimer binding energies as a function of interplanar spacing for chromophores **FMC**, **HMC**, and **TMC-2.** It can be seen that the binding at moderate-to-large intermolecular spacings is, not surprisingly, dominated by electrostatic dipole–dipole interactions. **TMC-2**, the most twisted and the most sterically encumbered chromophore of the series, is identified as having the greatest equilibrium intermolecular distance of 5.81 Å, with a computed dimer stabilization energy of $\Delta E_D = -42.3$ kcal/mol. Decreased twist angle, smaller dipole moment, and more favorable $\pi-\pi$ stacking results in an equilibrium packing distance of 4.1 Å for **FMC**. However, the lower dipole moment results in a reduced dimer stabilization energy of $\Delta E_D = -29.8$ kcal/mol, 30% less than for **TMC-2**. As the dimers are incrementally separated, there is a dramatic loss of stabilization which finally approaches zero, at which point the molecules no longer "sense" one another. It is important to note that by ~15 Å interplanar separation, the stabilization energies (ΔE_D) reach an asymptote near −5 kcal/mol (Figure 6). This nonzero asymptote may reflect basis set superposition error (BSSE),[25] arising from artificial lowering of the dimer energy due to basis set incompleteness. Since each of these calculations was carried out in the gas-phase, neglecting solvent stabilization effects, an additional calculation was carried out on **TMC-2** and **FMC** at their closest interplanar distances, to correct for the differential effects that solvation would have on each dimer. This was achieved using solvation/dimerization correction energies (ΔE_{sol}^{corr}; see Table 9).

In the absence of solvation, the **TMC-2** and **FMC** dimers (Table 9 and Figure 6), as explained previously, differ in energy by approximately 30%, with the **TMC-2** dimer being more stable. However, using a Poisson–Boltzmann scheme (see Experimental Section for details) in CH_2Cl_2, the **TMC-2** dimer

TABLE 4: PGSE-Derived Structural Parameters[a], for Both Monomers and Dimers, and Estimated Dimerization Equilibrium Constants for Chromophores FMC, DFMC, and TMC-2 in CH_2Cl_2[b]

	P_M	P_D	a_M	b_M	L	a_D	b_D	K_D^{PGSE}	$K_D^{^1H\ NMR}$
FMC	29.47	43.13 ± 2.27	10.5	3.5	11	15.5	4.5 ± 0.5	293 ± 149	215 ± 24
DFMC	37.90	57.73 ± 2.94	13.5	4.1	11	21.5	5.3 ± 0.6	189 ± 65	264 ± 47
TMC-2	31.65	56.24 ± 17.94	10.5	3.9	11	15.5	7.2 ± 4.0	203 ± 330	141 ± 62

[a] P_M, P_D, a_M, b_M, L, a_D, and b_D values are in Å. [b] K_D values are in M^{-1}. For parameters derived from best fits, error intervals are given at 95% confidence. K_D^{PGSE} values are derived from best fits to the PGSE data using eq 10. $K_D^{1}H$ NMR values are derived from dimerization-induced displacement of ^1H NMR chemical shifts.[24] Experimental data and nonlinear fitting analyses are reported in the Supporting Information. The K_D^{PGSE} and $K_D^{1}H$ NMR values are in agreement.

TABLE 5: EFISH Derived $\mu\beta$ Values for Chromophores FMC and DFMC as a Function of Concentration in CH_2Cl_2 at 1907 nm

samples	concentration (M)	$\mu\beta$ (10^{-48} esu)
FMC	1.5×10^{-3}	−2240 ± 90
	5×10^{-4}	−3120 ± 250
	1×10^{-4}	−4600 ± 1400
DFMC	1×10^{-3}	−2130 ± 100
	5×10^{-4}	−2340 ± 330
	5×10^{-5}	−2360 ± 5200
TMC-2[a]	1×10^{-3}	−436 ± 65
	9.6×10^{-4}	−872 ± 100
	1.1×10^{-4}	−14400 ± 2700
	5.0×10^{-5}	−19000 ± 3000
	1.0×10^{-5}	−22000 ± 2900
	5.0×10^{-6}	−24000 ± 2400

[a] From refs 10c and 10d.

TABLE 6: Computed Chromophore Structural and Electronic Structural Properties Associated with Increasing Methyl Substitution at the Arene−Arene Juncture and Arene−Arene Torsional Angle in TICT Chromophore Series FMC, HMC, and TMC-2

systems	twist angle (deg)	μ_g (D)	$\Delta\mu$ (D)	β (10^{-30}esu)	$\mu\beta$[a] (10^{-48} esu)
FMC	5.1	14.1	−6.5	109	−1540
HMC	40.2	23.1	−12.3	237	−5470
TMC-2	68	29.8	−21.4	518	−15400

[a] The sign of $\mu\beta$ is negative because μ and β are vectors, and are aligned in opposite directions.

TABLE 7: Comparison of Computed Chromophore Electronic Properties Associated with Increasing Methyl Substitution at the Arene−Arene Juncture and Increasing the Environmental Effective Dielectric Constant for the TICT Chromophore Series FMC, HMC, and TMC-2

	in gas phase ($F = 0$ au)		in CH_2Cl_2 ($F = 0.006$ au)	
systems	μ_g (D)	$\mu\beta$ (10^{-48} esu)	μ_g (D)	$\mu\beta$ (10^{-48} esu)
FMC	14.1	− 1540	15.2	− 1779
HMC	23.1	− 5470	24.3	− 7133
TMC-2	29.8	− 15400	33.1	− 18282

is now found to be less stable (ΔE_{sol}^{corr}) with respect to the **FMC** dimer. Using eq 6, the ΔE_{sta} values are now found to be −31.96 and −28.11 kcal/mol, respectively, with only a 12% difference between the two. This decrease in relative energies suggests that **FMC** and **TMC-2** will undergo aggregation in a similar fashion when solvated in moderately polar media such as CH_2Cl_2. This is in good agreement with the PGSE NMR data (see above). A qualitative state correlation diagram for these results is summarized in Figure 7.

Discussion

Compared to the synthesis of **TMC-2**, a major modification in the synthesis of chromophores **FMC** and **DFMC** is that the deprotonated form, the sodium salt of 2-(4-pyridin-4-yl-phenyl)malononitrile, instead of the protonated form, is used as the precursor for regioselective N-alkylation to afford chromophores **FMC** and **DFMC.** This is because of the following: (1) the sodium salts can be readily purified via recrystallization from water instead of using flash column chromatography, and, more importantly, (2) the protonated form of 2-(4-pyridin-4-ylphenyl)malononitrile is almost insoluble in most organic solvents, making it unsuitable for subsequent N-alkylation.

As discussed in Results, the difference between the crystal structures of **FMC** and **TMC-2** reveals a major change in electronic structure with reduced twist angle. Given that the (ring)C−C(ring) distance in **TMC-2** (1.488(5) Å) is only slightly

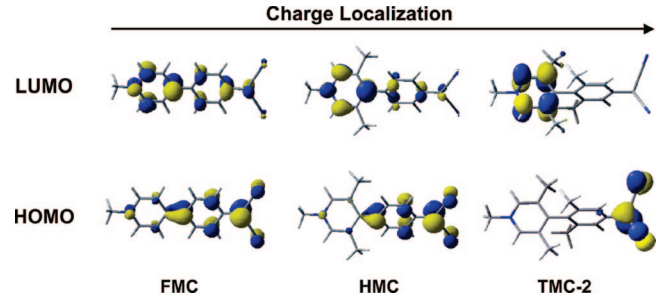

Figure 5. Isodensity surface plots of the HOMOs and LUMOs of chromophores **FMC**, **HMC**, and **TMC-2**. Note increasing charge localization with enforced twist angle.

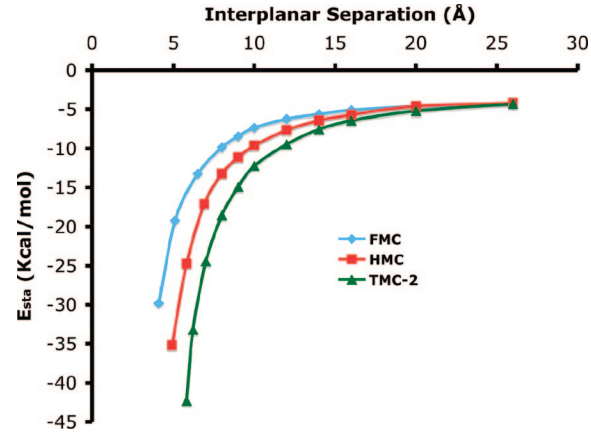

Figure 6. Computed dimerization energies for unsolvated TICT chromophores **FMC**, **HMC**, and **TMC-2** as a function of ring–ring interplanar separation in the structures given in Chart 2B at the RHF/3-21G* level.

TABLE 8: DFT Optimized Structural Data for Chromophores with Increasing Steric Interactions

chromophore	ipso (ring)C−C(ring) (Å)	(ring)C−C$(CN)_2$ (Å)
FMC	1.418	1.407
HMC	1.438	1.413
TMC-2	1.468	1.426

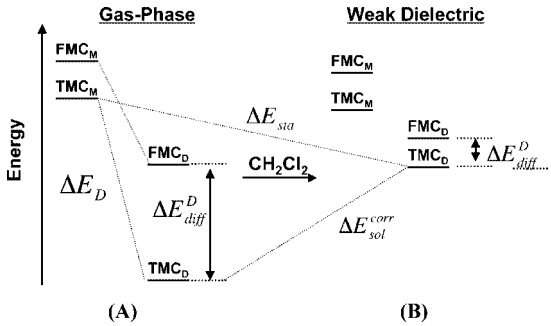

Figure 7. Qualitative state correlation diagram (M = monomer, D = dimer) as a function of twist angle and solvent polarity. (A) Gas-phase energetics showing the stability of **TMC-2** vs **FMC**. (B) Poisson–Boltzmann continuum model with CH_2Cl_2 as the solvent. Upon increasing the surrounding polarity, there is a stabilization of monomers relative to dimers and destabilization of the **TMC-2** dimer relative to the **FMC** dimer.

TABLE 9: Energetics of Dimerization, Solvation with Dimer Relaxation, and the Total Stabilization for Chromophores FMC and TMC-2

chromophore	ΔE_D(kcal/mol)	ΔE_{sol}^{corr}(kcal/mol)	ΔE_{sta}(kcal/mol)
FMC	− 29.8	1.69	− 28.11
TMC-2	− 42.3	10.34	− 31.96

longer than in typical biaryls (~1.487 Å),[26] the significantly shortened (ring)C−C(ring) distance in **FMC** (1.449(6) Å) strongly argues for an increased contribution from a quinoidal structure in the ground state.[10a,b] The same is true for the shortened (ring)C−C$(CN)_2$ distance in **FMC** (1.429(6) Å) vs that in **TMC-2** (1.463(5) Å). These structural results are consistent not only with a smaller computed **FMC** ground-state dipole moment (Table 6; μ = 14.1 D in **FMC** vs 29.8 D in **TMC-2**) but also with a smaller change in dipole moment ($\Delta\mu$) from the ground to first charge-separated excited state (Table 6). The latter description is also supported by smaller solvatochromic shifts observed in the optical spectroscopy (Table 2). In addition, the EFISH measurements reveal a dramatic decrease in β with decreased dihedral angle twist (**TMC-2** → **FMC** in Table 5) which is also consistent with the results of the present theoretical calculations (Table 6) and with those for other TICT chromophores with different molecular architectures and at different levels of computation.[9,10a–,d]

The documented tendency of TICT chromophores such as **TMC-2** and **TMC-3** to undergo electrostatic self-aggregation in nonpolar or relatively nonpolar solvents (but much less in polar solvents)[10c,d] is also observed in the present study by PGSE NMR, EFISH, and computation using the Poisson–Boltzmann solvation continuum model (Tables 3, 5, and 9). Our experimental results here reveal that although the **FMC** chromophores have smaller dipole moments in comparison to **TMC-2**, this is balanced by the more planar structures so that the thermodynamics of aggregation are virtually identical in CH_2Cl_2 (Figure 8). These results are also in good agreement with the theoretical results (Table 9 and Figure 7). Clearly those factors which favor or oppose aggregation are subtle but should be controllable by appropriate TICT chromophore functionalization.

Conclusions

The reduced twist angle TICT chromophore **FMC** was designed, synthesized, and characterized. The crystallographic data reveal a much smaller dihedral twist angle in **FMC** than in the highly twisted analogue, **TMC-2**. The pronounced shortening of the (ring)C−C(ring) and (ring)C−C$(CN)_2$ distances is in accord with a dramatic change in electronic structure: increased contribution from a quinoidal structure in the ground state of **FMC** rather than the dominant zwitterionic structure of **TMC-2**. However, similar to **TMC-2**, negative solvatochromism is observed in optical absorption spectra, and a negative sign of the $\mu\beta$ value is obtained from the EFISH measurements, indicating a similar NLO response mechanism. In addition, as predicted by theoretical calculations, the less twisted **FMC** chromophores have much smaller molecular hyperpolarizabilities. All these results not only provide strong support for our previously proposed EO response mechanism of TICT chromophores[10a,c] but also reveal the relationship between molecule hyperpolarizabilty and the dihedral twist angle. These results provide new insights into how simple optimization of chromophore molecular structure can be used to maximize molecular hyperpolarizability by adjusting key metrical parameters.

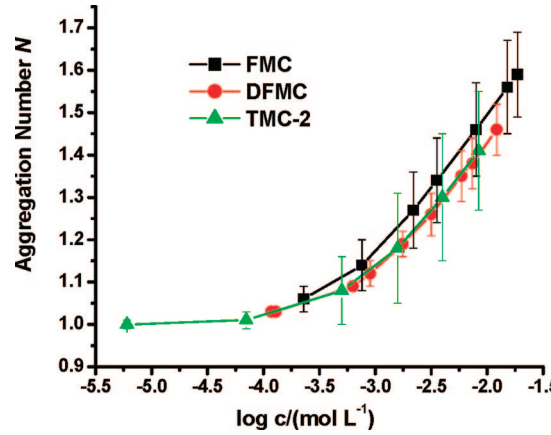

Figure 8. PGSE NMR derived aggregation number (from Table 3) as a function of concentration for chromophores **FMC**, **DFMC**, and **TMC-2** in CD_2Cl_2 solution.

The basically similar solution-phase aggregation behavior observed for chromophores **FMC** and **DFMC** versus **TMC-2** via concentration-dependent EFISH and PGSE measurements indicates that even though the former have smaller dipole moments than **TMC-2**, that should in principle disfavor self-aggregation, the structural data reveal that a detuned chromophore structure allows shorter interplanar approaching distances and leads to stable face-to-face stacking.

Acknowledgment. T.J.M. and M.A.R. thank DARPA/ONR (Grant SP01P7001R-A1/N00014-00-C) and the NSF-Europe program (Grant DMR-0353831) for support of this research, and the Northwestern University NSF MRSEC for support of characterization facilities (Grant DMR-0520513). E.C. and R.U. thank the MIUR (FIRB 2003 "Molecular compounds and hybrid nanostructured materials with resonant and non-resonant optical properties for photonic devices") for support of EFISH measurements. This paper is dedicated to Larry Dalton, friend, colleague, and scholar.

Supporting Information Available: Crystallographic data (CIF) and PGSE data (PDF). This material is available free of charge via the Internet at http://pubs.acs.org.

References and Notes

(1) (a) Dalton, L. R. In *Handbook of Conducting Polymers*; Skotheim, T. A.; Reynolds, J. R., Eds.; CRC Press: Boca Raton, FL, 2007; Chapter 2. (b) Kim, T.-D.; Kang, J.-W.; Luo, J.; Jang, S.-H.; Ka, J.-W.; Tucker, N.; Benedict, J. B.; Dalton, L. R.; Gray, T.; Overney, R. M.; Park, D. H.;

Herman, W. N.; Jen, A. K.-Y. *J. Am. Chem. Soc.* **2007**, *129*, 488. (c) Dalton, L. R.; Sullivan, P. A.; Bale, D. H.; Olbricht, B. C. *Solid-State Electron.* **2007**, *51*, 1263. (d) Rommel, H. L.; Robinson, B. H. *J. Phys. Chem. C* **2007**, *111*, 18765. (e) DeRose, C. T.; Enami, Y.; Loychik, C.; Norwood, R. A.; Mathine, D.; Fallahi, M.; Peyghambarian, N.; Luo, J. D.; Jen, A. K.-Y.; Kathaperumal, M.; Yamamoto, M. *Appl. Phys. Lett.* **2006**, *89*, 131102. (f) Marder, S. R. *Chem. Commun. (Cambridge)* **2006**, 131. (g) Locatelli, D.; Quici, S.; Roberto, D.; De Angelis, F. *Chem. Commun. (Cambridge)* **2005**, 5405. (h) Baehr-Jones, T.; Hochberg, M.; Wang, G.; Lawson, R.; Liao, Y.; Sullivan, P. A.; Dalton, L.; Jen, A. K. Y.; Scherer, A. *Opt. Express* **2005**, *13* (14), 5216. (i) Sinyukov, A. M.; Leahy, M. R.; Hayden, L. M.; Haller, M.; Luo, J.; Jen, A. K. Y.; Dalton, L. R. *Appl. Phys. Lett.* **2004**, *85* (24), 5827. (j) Dalton, L. R. *Pure Appl. Chem.* **2004**, *76*, 1421. (k) Kajzar, F.; Lee, K.-S. A.; Jen, K.-Y. *Adv. Polym. Sci.* **2003**, *161*, 1. (l) Dalton, L. R. *Adv. Polym. Sci.* **2002**, *158*, 1. (m) Shi, Y.; Zhang, C.,.; Bechtel, J. H.; Dalton, I. R.; Robinson, B. H.; Steier, W. H. *Science* **2000**, *288*, 119. (n) Kuzyk, M. G. *Phys. Rev. Lett.* **2000**, *85* (6), 1218. (o) Zyss, J. Special Issue: Molecular Nonlinear Optics: Materials, Phenomena and Devices. *Chem. Phys.* **1999**, 245. (p) Verbiest, T.; Houbrechts, S.; Kauranen, M.; Clays, K.; Persoons, A. *J. Mater. Chem.* **1997**, *7*, 2175. (q) Marder, S. R.; Kippelen, B.; Jen, A. K. Y.; Peyghambarian, N. *Nature* **1997**, *388*, 845. (r) Marks, T. J.; Ratner, M. A. *Angew. Chem., Int. Ed. Engl.* **1995**, *34*, 155.

(2) (a) Liao, Y.; Bhattacharjee, S.; Firestone, K. A.; Eichinger, B. E.; Paranji, R.; Anderson, C. A.; Robinson, B. H.; Reid, P. J.; Dalton, L. R. *J. Am. Chem. Soc.* **2006**, *128*, 6847. (b) Datta, A.; Pati, S. K. *Chem.-Eur. J.* **2005**, *11*, 4961. (c) Coe, B. J.; Jones, L. A.; Harris, J. A.; Brunschwig, B. S.; Asselberghs, I.; Clays, K.; Persoons, A.; Garin, J.; Orduna, J. *J. Am. Chem. Soc.* **2004**, *126*, 3880. (d) Abbotto, A.; Beverina, L.; Bradamante, S.; Facchetti, A.; Klein, C.; Pagani, G. A.; Redi-Abshiro, M.; Wortmann, R. *Chem.-Eur. J.* **2003**, *9*, 1991. (e) Barlow, S.; Marder, S. R. *Chem. Commun. (Cambridge)* **2000**, 1555. (f) Jen, A. K.-Y.; Ma, H.; Wu, X.; Wu, J.; Liu, S.; Marder, S. R.; Dalton, L. R.; Shu, C.-F. *SPIE Proc.* **1999**, *3623*, 112.

(3) (a) Isborn, C. M.; Leclercq, A.; Vila, F. D.; Dalton, L. R.; Bredas, J. L.; Eichinger, B. E.; Robinson, B. H. *J. Phys. Chem. A* **2007**, *111*, 1319. (b) Qudar, J. L.; Chemla, D. S. *J. Chem. Phys.* **1977**, *66*, 2664. (c) Marder, S. R.; Beratan, D. N.; Cheng, L.-T. *Science* **1991**, *252*, 103. (d) Albert, I. D. L.; Marks, T. J.; Ratner, M. A. First Hyperpolarizability of Molecular Chromophores: Practical Computational Approaches. In *Progress in Organic Nonlinear Optics*; Kuzyk, M., Dirk, C. R., Eds.; Marcel Dekker: New York, 1998; pp 37−109. (e) Albert, I. D. L.; Marks, T. J.; Ratner, M. A. *ACS Symposium Series* **1996**, *628*, 116–135. (f) Kanis, D. R.; Ratner, M. A.; Marks, T. J. *Chem. Rev.* **1994**, *94*, 195–242.

(4) (a) Cariati, E.; Macchi, R.; Roberto, D.; Ugo, R.; Galli, S.; Casati, N.; Macchi, P.; Sironi, A.; Bogani, L.; Caneschi, A.; Gatteschi, D. *J. Am. Chem. Soc.* **2007**, *129*, 9410. (b) Lee, J.-Y.; Kim, J.-H.; Jung, W.-T. *Mol. Cryst. Liq. Cryst.* **2007**, *471*, 347. (c) Bidault, S.; Brasselet, S.; Zyss, J.; Maury, O.; Le Bozec, H. *J. Chem. Phys.* **2007**, *126*, 034312/1. (d) Maury, O.; Le Bozec, H. *Acc. Chem. Res.* **2005**, *38*, 691. (e) Chang, C.-C.; Chen, C.-P.; Chou, C.-C.; Kuo, W.-J.; Jeng, R.-J. *J. Macromol. Sci., Polym. Rev.* **2005**, *C45*, 125. (f) Qin, A.; Yang, Z.; Bai, F.; Ye, C. *J. Polym. Sci., Part A: Polym. Chem.* **2003**, *41*, 2846.

(5) Alias, S.; Andreu, R.; Blesa, M. J.; Franco, S.; Garin, J.; Gragera, A.; Orduna, J.; Romero, P.; Villacampa, B.; Allain, M. *J. Org. Chem.* **2007**, *72*, 6440. (b) Andreu, R.; Blesa, M. J.; Carrasquer, L.; Garin, J.; Orduna, J.; Villacampa, B.; Alcala, R.; Casado, J.; Ruiz, D.; Mari, C.; Lopez Navarrete, J. T.; Allain, M. *J. Am. Chem. Soc.* **2005**, *127*, 8835. (c) Marder, S. R.; Kippelen, B.; Jen, A. K.-Y.; Peyghambarian, N. *Nature* **1997**, *388*, 845. (d) Marder, S. R.; Cheng, L. T.; Tiemann, B. G.; Friedli, A. C.; Blanchard-Desce, M.; Perry, J. W.; Skindhoej, J. *Science* **1994**, *263*, 511. (e) Marder, S. R.; Gorman, C. B.; Tiemann, B. G.; Cheng, L. T. *J. Am. Chem. Soc.* **1993**, *115*, 2524.

(6) (a) Albert, I. D. L.; Marks, T. J.; Ratner, M. A. *Chem. Mater.* **1998**, *10*, 753. (b) Albert, I. D. L.; Marks, T. J.; Ratner, M. A. *J. Am. Chem. Soc.* **1997**, *119*, 6575.

(7) (a) Dragonetti, C.; Righetto, S.; Roberto, D.; Ugo, R.; Valore, A.; Fantacci, S.; Sgamellotti, A.; De Angelis, F. *Chem. Commun. (Cambridge)* **2007**, *40*, 4116. (b) Traber, B.; Wolff, J. J.; Rominger, F.; Oeser, T.; Gleiter, R.; Goebel, M.; Wortmann, R. *Chem.-Eur. J.* **2004**, *10*, 1227. (c) Kang, H.; Zhu, P.; Yang, Y.; Facchetti, A.; Marks, T. J. *J. Am. Chem. Soc.* **2004**, *126*, 15974. (d) Yang, M.-L.; Champagne, B. *J. Phys. Chem. A* **2003**, *107*, 3942. (e) Ostroverkhov, V.; Petschek, R. G.; Singer, K. D.; Twieg, R. J. *Chem. Phys. Lett.* **2001**, *340*, 109.

(8) (a) Tripathy, K.; Moreno, J. P.; Kuzyk, M. G.; Coe, B. J.; Clays, K.; Kelley, A. M. *J. Chem. Phys.* **2004**, *121*, 7932. (b) Kuzyk, M. G. *Phys. Rev. Lett.* **2000**, *85* (6), 1218.

(9) (a) Keinan, S.; Zojer, E.; Bredas, J.-L.; Ratner, M. A.; Marks, T. J. *J. Mol Struct. (THEOCHEM)* **2003**, *633*, 227. (b) Albert, I. D. L.; Marks, T. J.; Ratner, M. A. *J. Am. Chem. Soc.* **1998**, *120*, 11174. (c) Albert, I. D. L.; Marks, T. J.; Ratner, M. A. *J. Am. Chem. Soc.* **1997**, *119*, 3155.

(10) (a) Brown, E. C.; Marks, T. J.; Ratner, M. A. *J. Phys. Chem. B* **2008**, *112*, 44–50. (b) Isborn, C. M.; Davidson, E. R.; Robinson, B. H. *J. Phys. Chem. A* **2006**, *110*, 7189. (c) Kang, H.; Facchetti, A.; Jiang, H.; Cariati, E.; Righetto, S.; Ugo, R.; Zuccaccia, C.; Macchioni, A.; Stern, C. L.; Liu, Z.; Ho, S.-T.; Brown, E. C.; Ratner, M. A.; Marks, T. J. *J. Am. Chem. Soc.* **2007**, *129*, 3267. (d) Kang, H.; Facchetti, A.; Zhu, P.; Jiang, H.; Yang, Y.; Cariati, E.; Righetto, S.; Ugo, R.; Zuccaccia, C.; Macchioni, A.; Stern, C. L.; Liu, Z.; Ho, S.-T.; Marks, T. J. *Angew. Chem., Int. Ed.* **2005**, *44*, 7922. (e) Kang, H.; Facchetti, A.; Stern, C. L.; Rheingold, A. L.; Kassel, W. S.; Marks, T. J. *Org. Lett.* **2005**, *7*, 3721.

(11) The chemical shifts of protons on zwitterionic chromophores in $CDCl_3$ are concentration-dependent because of the dimerization.

(12) Tanner, J. *J. Chem. Phys.* **1970**, *52*, 2523.

(13) Mills, R. *J. Phys. Chem.* **1973**, *77*, 685. Data at different temperatures were estimated by interpolation of the data reported by Mills, giving $D_{HDO} = 1.780 \times 10^{-9}$ m^2 s^{-1} at 295.7 K

(14) (a) The viscosity of CD_2Cl_2 was estimated to be 0.4256 cP at 295.7 K by interpolation of the data reported for CH_2Cl_2: *CRC Handbook of Chemistry and Physics*, 67th ed.; Weast, R. C., Ed.; CRC Press: Cleveland, OH, 1986. (b) The viscosity was corrected for the reduced mass as proposed by Holz et al.: Holz, M.; Mao, X.; Seiferling, D.; Sacco, A. *J. Chem. Phys.* **1996**, *104*, 669. (c) The viscosity of DMSO-d_6 was estimated to be 2.138 cP at 295.7 K by interpolation of the data reported for DMSO: Higashigaki, Y.; Christensen, D. H.; Wang, C. H. *J. Phys. Chem.* **1981**, *85*, 2531. (d)It was corrected for the reduced mass as proposed by Holz et al.[10b]

(15) Zuccaccia, D.; Macchioni, A. *Organometallics* **2005**, *24*, 3476.

(16) Jaguar. *Jaguar 4.2*; Schrödinger: Portland, OR, 1991–2000.

(17) (a) Becke, A. D. *Phys. Rev. A* **1988**, *38*, 3098. (b) Lee, C.; Yang, W.; Parr, R. G. *Phys. Rev. B* **1988**, *37*, 785.

(18) *Spartan '06*; Wavefunction: Irvine, CA, 2006.

(19) Nicholls, A.; Honig, B. *J. Comput. Chem.* **1991**, *12*, 435.

(20) Ridley, J.; Zerner, M. *Theor. Chim. Acta* **1973**, *32*, 111.

(21) Zeng, J.; Hush, N. S.; Reimers, J. R. *J. Am. Chem. Soc.* **1996**, *118*, 2059.

(22) Orr, B. J.; Ward, J. F. *Mol. Phys.* **1971**, *20*, 513.

(23) Macchioni, A.; Ciancaleoni, G.; Zuccaccia, C.; Zuccaccia, D. *Chem. Soc. Rev.* **2008**, *37*, 479.

(24) Martin, R. B. *Chem. Rev.* **1996**, *96*, 3043.

(25) Jensen, F. *Introduction to Computational Chemistry*; John Wiley & Sons: West Sussex, England, 1999.

(26) Allen, F. H.; Kennard, O.; Watson, D. G.; Brammer, L.; Orpen, A. G.; Taylor, R. Database of average bond lengths in organic compounds. *J. Chem. Soc., Perkin Trans. 2* **1987**, S1.

JP8003135